EVALUATING THE EFFECTS OF SPACE WEATHERING ON ASTEROIDAL ACCESSORY PHASES: MAGNETITE AND PENTLANDITE. L. C. Chaves[1], M. S. Thompson[1], C. A. Dukes[2], M. J. Loeffler[3], B. Horgan[1]., P. S. Szabo[4], N. L. Smith[2], K. D. Ardrey[2]. [1]Department of Earth, Atmospheric, and Planetary Sciences, Purdue University, 550 Stadium Mall Drive, West Lafayette, IN, 47907. lchavesm@purdue.edu. [2]Laboratory for Astrophysics and Surface Physics, University of Virginia, 351 McCormick Road, Charlottesville, VA 22904, [3]Department of Physics and Astronomy, Northern Arizona University, 527 S. Beaver St, Flagstaff, AZ, 86011. [4]Space Sciences Laboratory, University of California, Berkeley, 7 Gauss Way, Berkeley, CA 94720, United States of America.

Introduction: Airless planetary surfaces are subjected to high-velocity micrometeoroid impacts and ion irradiation from the solar wind through a process known as space weathering [1]. Space weathering alters the chemistry, microstructure, and spectral properties of mineral grains on airless surfaces. Studies of returned samples and experiments simulating space weathering in the laboratory have focused on silicate minerals, the major components of lunar soils. However, as space weathering studies have expanded to include the analysis of samples from other planetary bodies, it is important to understand the contribution of their different mineral constituents to the broader spectral characteristics of these planetary surfaces. Some understudied mineral phases include Fe-oxides and Fe-sulfides, which are important accessory minerals in carbonaceous meteorites, are present in the sample collection from asteroid Itokawa and Ryugu, and have been identified on the surface of asteroid Bennu through remote sensing observations [2-5]. However, few efforts have been made to understand how these minerals are altered by exposure to the interplanetary space environment [6,7]. Here we simulate micrometeoroid bombardment and solar wind irradiation on magnetite and pentlandite using pulsed laser and ion irradiation, respectively. Their spectral, chemical, and structural properties are characterized using coordinated analytical techniques.

Methods: We obtained Fe_3O_4 powders with 99.9% purity, sieved them to <45 μm particle size, and pressed them into pellets using Al holders at 1500 psi. To simulate micrometeoroid bombardment on magnetite, we irradiated our sample under vacuum ($5x10^{-8}$ Torr) with a Nd-YAG laser that has a pulse width of 4-6 ns and energy of 3.5 mJ per pulse. To evaluate the reflectance response of magnetite under pulsed laser irradiation, we conducted in situ reflectance spectroscopy measurements in the visible near-infrared (VNIR) region (0.3-2.5μm) using Avantes AvaSpec 2048XL and Thermo Scientific Nicolet iS50 spectrometers at pre-specified intervals during the irradiation.

To analyze the response of magnetite under solar wind irradiation, we conducted 1 keV H^+ irradiation using a flux of $1.2x10^{13}$ ions/cm^2/s up to a total fluence of $8.68x10^{17}$ H^+/cm^2, and 4 keV He^+ irradiation with a flux of $9.1x10^{12}$ He^+/cm^2/s up to a total fluence of $3.6x10^{16}$ He^+/cm^2. To evaluate changes in chemistry due to ion irradiation, we performed X-ray photoelectron spectroscopy (XPS) using a PHI Versaprobe III equipped with an Al K∝ X-ray source. Additionally, we used SDTrimSP models in dynamic mode to understand chemical changes in magnetite induced by ion irradiation. In order to characterize the morphological changes on magnetite produced by laser and ion irradiation, we prepared electron transparent thin sections with a Thermo Scientific Helios G4 UX DualBeam focused ion beam scanning electron microscope at Purdue University. These thin sections were analyzed using a 200 keV FEI Talos transmission electron microscope (TEM) equipped with an energy dispersive X-ray spectroscopy (EDS) system.

For pentlandite synthesis, we used a similar technique as [8,9]. We acquired Fe, Ni, and S powders from Sigma Aldrich with a purity > 99% that were weighted to provide a $Fe_{4.5}Ni_{4.5}S_8$ formula and mixed using mortar and pestle under an inert environment to reduce oxidation. The mixture was encapsulated in a 1 cm diameter quartz tube and inserted into a box furnace, where it was slowly heated to 700°C and maintained for 3h. Subsequently, the temperature was increased to 1100°C for 10 h before the samples were allowed to cool down to room temperature. We will conduct the same pulsed laser and ion irradiation experiments on pentlandite as described for magnetite.

Results: Several morphological, chemical, microstructural, and spectral modifications for magnetite were identified after the irradiation experiments.

Scanning electron microscopy. Analyses were performed for the H^+ and He^+ irradiated pellets. However, no differences were identified between the non-irradiated and irradiated regions of the pellets. In contrast, the pulsed laser irradiated magnetite shows the development of widespread melts on the surface.

Reflectance Spectroscopy. Measurements of the laser irradiated magnetite across the VNIR wavelengths reveal an increase in reflectance with increasing pulses up to 3x. However, after 5x, the reflectance decreases.

1 keV H^+ and 4 keV He^+ irradiation. Survey XPS data exhibit a depletion of O and enrichment of Fe with increasing ion fluence. Before irradiation, the

concentrations were 45 at% Fe and 55 at% O, and after the final fluence of 8.59x10^{17} H$^+$/cm^2 these concentrations changed to 83 at% and 17 at%, respectively. Fe enrichment and O depletion were also identified as a result of 4 keV He$^+$ irradiation. The initial concentrations were 44 at% Fe and 56 at% O, and after a final fluence of 3.6 x 10^{16} He$^+$/cm^2, the concentrations were 53 at% and 47 at%, respectively.

SDTrimSP simulations. SDTrimSP models were conducted for comparison to the XPS survey data and to identify chemical changes resulting from ion irradiation. For 1 keV H$^+$ irradiation we used initial concentrations of 43 at% Fe and 57 at% O, and after the final fluence these changed to 79 at% Fe and 21% O. In addition, for the 4 keV He$^+$ irradiation, the concentrations varied from 44 at% to 57 at % for Fe, and from 56 at% to 43 at% for O. The results obtained by the simulations are in excellent agreement with the Fe and O concentrations obtained by XPS (Fig. 1).

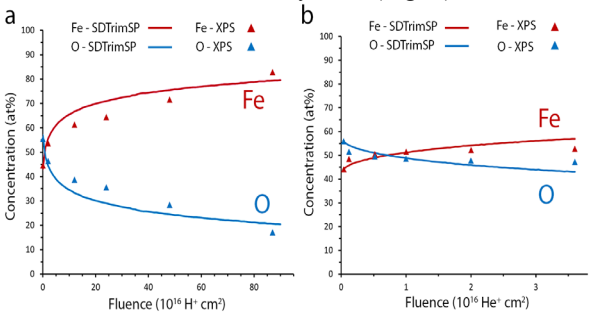

Figure 1. Fe and O concentrations on magnetite after ion irradiation. a) 1 keV H$^+$, b) 4 keV He$^+$

Transmission Electron Microscopy. Bright field (BF) TEM imaging of the magnetite irradiated with 1 keV H$^+$ reveals the presence of a 30 nm rim on the outer surface. This rim is crystalline, as shown by high-resolution (HR) TEM images, and exhibits lattice fringes with d-spacing values of 2.0 Å, corresponding to metallic iron. EDS maps show that this rim is enriched in Fe and depleted in O compared to the underlying magnetite. Similarly, the magnetite irradiated with 4 keV He$^+$ has a 50 nm crystalline rim that contains elongated defects with no chemical changes identified by EDS.

The magnetite irradiated 5x with the pulsed laser has a 160 nm thick dual-layer rim (Fig. 2) that corresponds to the melt identified by the SEM. The outer layer is crystalline and the inner layer is a combination of crystalline and amorphous material. No chemical differences between the melt and the underlying magnetite were identified by EDS.

Discussion: Fe enrichment and O depletion were identified in magnetite after 1 keV H$^+$ and 4 keV He$^+$

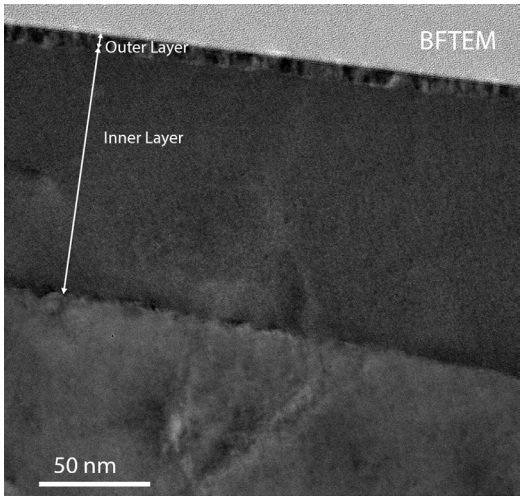

Figure 2. Transmission electron microscopy image of magnetite after 5 laser pulses.

with both XPS analysis and SDTrimSP models. This chemical behavior is attributed to a preferential sputtering of O, as it has a lower binding energy compared to Fe [10], and to damage-driven diffusion effects. EDS and HRTEM analysis of the H$^+$ irradiated magnetite reveal the formation of a metallic iron rim. XPS analysis and SDTrimSP models revealed a depletion of O in the outer 5 nm in magnetite as a result of He$^+$ irradiation. However, no chemical change was identified by EDS. This discrepancy could be caused by rapid oxidation due to atmospheric exposure prior to TEM analysis.

In addition, the XPS and TEM analyses for the pulsed laser and ion irradiation experiments on the synthetic pentlandite are underway and will be presented at the meeting.

References: [1] Pieters C. M. and Noble S. K. (2016) *J. Geophys. Res. Planets, 121*, 1865–1884. [2] Bland P. A. et al. (2012) *Meteoritics & Planet. Sci., 39,* 3-16. [3] Nakamura T. et al. (2011) *Science, 333,*1113-1116. [4] Yokoyama T. et al. (2022) *Science, 1-18.* [5] Lauretta D. S. et al. (2019) *Nature,* 568, 55-60. [6] Christoffersen R. and Keller L. P. (2011) *Meteoritics & Planet. Sci., 46,* 950-969. [7] Chaves L. C. and Thompson M.S. (2022) *Earth, Planets and Space, 74:124,* 1-14. [8] Drebushchak V. A. et al. (1998) *J. Cryst. Growth, 193,* 728-731. [9] Puring K. J. et al. (2017) *J. Vis. Exp., 124,* e56087. [10] McIntyre N. S. and Zetaruk D. G. (1977) *Anal. Chem.* 49, 1521-1529.